Applied Physics Letters

The magnetic P-T phase diagram of langasite $Ba_3TaFe_3Si_2O_{14}$ at high hydrostatic pressures up to 38 GPa

Cite as: Appl. Phys. Lett. **103**, 162402 (2013); https://doi.org/10.1063/1.4822422
Submitted: 19 July 2013 . Accepted: 04 September 2013 . Published Online: 14 October 2013

A. G. Gavriliuk, I. S. Lyubutin, S. S. Starchikov, A. A. Mironovich, S. G. Ovchinnikov, I. A. Trojan, Yuming Xiao, Paul Chow, S. V. Sinogeikin, and V. V. Struzhkin

The magnetic P-T phase diagram of langasite $Ba_3TaFe_3Si_2O_{14}$ at high hydrostatic pressures up to 38 GPa

A. G. Gavriliuk,[1,2,3,a)] I. S. Lyubutin,[2,b)] S. S. Starchikov,[2] A. A. Mironovich,[3] S. G. Ovchinnikov,[4,5] I. A. Trojan,[2] Yuming Xiao,[6] Paul Chow,[6] S. V. Sinogeikin,[6] and V. V. Struzhkin[1]

[1]*Geophysical Laboratory, Carnegie Institution of Washington, 5251 Broad Branch Road NW, Washington DC 20015, USA*
[2]*Institute of Crystallography, Russian Academy of Sciences, Leninsky prospekt 59, Moscow 119333, Russia*
[3]*Institute for Nuclear Research, Russian Academy of Sciences, 60-letiya Oktyabrya prospekt 7a, Moscow 117312, Russia*
[4]*L. V. Kirensky Institute of Physics, Siberian Branch of Russian Academy of Sciences, Krasnoyarsk 660036, Russia*
[5]*Siberian Federal University, 79 Svobodny Prospect, Krasnoyarsk 660041, Russia*
[6]*High Pressure Collaborative Access Team, Geophysical Laboratory, Carnegie Institution of Washington, Argonne, Illinois 60439, USA*

(Received 19 July 2013; accepted 4 September 2013; published online 14 October 2013)

The langasite-type crystals with 3d ions are considered as a class of multiferroics in which ferroelectricity can be induced by the magnetic ordering. In this paper, the high-pressure magnetic states of the langasite-type powdered sample $Ba_3TaFe_3Si_2O_{14}$ have been investigated in a diamond anvil cell by the nuclear forward scattering of synchrotron radiation technique at different temperatures in hydrostatic conditions. In the pressure range of $0 < P < 19.5$ GPa, an increase of the Neel temperature T_N from 27 to 41 K was observed in the antiferromagnetic phase of the material. At pressures ~19.5 GPa, a transition to another magnetic phase with huge increase in the Neel temperature to ~120 K was found. We attribute this change to the structural transition at ~19.5 GPa which is evidenced by a drastic change of Raman spectra at this pressure. A tentative magnetic P-T phase diagram of $Ba_3TaFe_3Si_2O_{14}$ is proposed. © *2013 AIP Publishing LLC*. [http://dx.doi.org/10.1063/1.4822422]

The $Ba_3TaFe_3Si_2O_{14}$ compound has the trigonal crystal structure of the $Ca_3Ga_2Ge_4O_{14}$ type (space group $P321$, $Z = 1$) and belongs to the iron containing langasite family.[1,2] Langasite $La_3Ga_5SiO_{14}$, which gave the name to the whole family, is a crystal with unique piezoelectric properties that exceed those of quartz, and it also has interesting combination of luminescent, laser, and nonlinear optical properties.[3] Crystal structure consists of tetrahedral layers, parallel to the *ab* plane, separated along the *c* axis with the layers consisting of oxygen octahedrons and large polyhedrons (Fig. 1).[1,4,5] The Fe^{3+} ions in the 3*f* tetrahedra form a net of triangle clusters on a hexagonal lattice in planes parallel to the *ab* plane (Fig. 1).[1]

The competition between intra-layer and interlayer super-exchange interactions leads to a frustrated magnetic structure,[6,7] which can result in the 120° spin arrangement in the triangle lattice of iron magnetic moments. Such 120° spin ordering in the iron triangles within *ab* layers was recently found in the neutron diffraction measurements of the similar compound $Ba_3NbFe_3Si_2O_{14}$.[7–9] When alternating the *ab* layers along the c axis, the iron moments of each triangle rotate by ≈51° forming a helical structure.[9] The detailed description of this magnetically ordered structure and its theoretical consideration can be found elsewhere.[10,11]

The splitting of crystallographic iron sites into two magnetic sublattices, which was found at $T < 27$ K by Mössbauer spectroscopy in the $Ba_3TaFe_3Si_2O_{14}$,[2,6] was associated with the structural phase transition induced by the magnetic ordering at ambient pressure. Depending on chemical composition, the correlation between the T_N value and the Mössbauer-spectra isomer shift *IS* was found, which reveals that T_N increases significantly with the strengthening covalence of Fe-O bonds in the 3*f* tetrahedral sites.[6] In particular, the T_N value for the compounds with Sb^{5+} ions in 1*a* octahedra is about 30% higher than in the compounds with Nb^{5+} and Ta^{5+}. Thus, one can expect strong pressure dependence

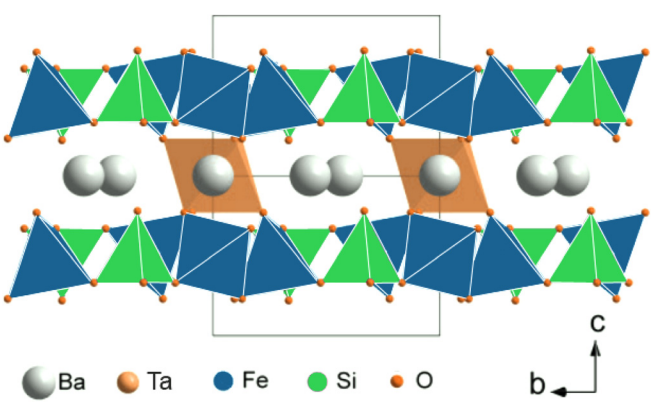

FIG. 1. The unit cell of the iron langasite $Ba_3TaFe_3Si_2O_{14}$ crystal structure of the $Ca_3Ga_2Ge_4O_{14}$ type (space group $P321$, $Z = 1$). The Fe^{3+} and Si^{4+} ions are inside of blue and green oxygen tetrahedrons, respectively. The Ba^{2+} ions (grey color) are in Thompson cubes (not shown), while Ta^{5+} ions are inside of yellow octahedrons.

[a)]Electronic mail: gavriliuk@mail.ru
[b)]Electronic mail: lyubutinig@mail.ru

of magnetic properties, in particular T_N, due to compression of Fe-O bonds.

It is shown below that the pressure-induced behavior of iron ions in the tetrahedral sites of the langasite-type compounds differs dramatically from their behavior in octahedral coordination, which was previously investigated in many strongly correlated transition metal oxides.[12–23]

In this work, polycrystalline langasite $Ba_3TaFe_3Si_2O_{14}$ compacts and powder samples have been studied under high pressure in a diamond-anvil cell[24] (DAC) by Raman spectroscopy and by the nuclear forward scattering (NFS) of synchrotron radiation (SR) in the temperature range of 20–300 K and at pressures from ambient to 38 GPa. The pressure dependence of the Neel temperature was calculated from the experimental data and magnetic P-T phase diagram was plotted and analysed.

Polycrystalline sample of the iron-containing langasite $Ba_3TaFe_3Si_2O_{14}$ was synthesized by the solid-phase sintering from compacted mixtures of corresponding salts and oxides. Iron in the sample was enriched with the ^{57}Fe isotope up to 50 wt. %, and the sample had deep yellow coloration. The phase composition was controlled by X-ray powder diffraction and by the transmission Mössbauer spectroscopy.[2] The lattice parameters of $Ba_3TaFe_3Si_2O_{14}$ are $a = 8.539(1)$ and $c = 5.234(1)$ Å^2.

For high-pressure experiments, polycrystalline compacts were squeezed between diamond anvils in DAC to form flat plates with the thickness 3–10 μm, which fits well the size of a pressure chamber. At room temperature, the $Ba_3TaFe_3Si_2O_{14}$ sample platelet with dimensions of about $70 \times 70 \times 3$ $(\mu m)^3$ was placed into DAC. The cullet size was about 270 μm and the diameter of the hole in the rhenium gasket where the sample was placed was about 120 μm. The pressure medium was He in the NFS experiment and Ne in the Raman scattering experiment, and it was clamped in DAC at pressure of about 2 kbar. A standard ruby fluorescence technique was used to measure pressure. Several ruby chips with dimensions of about 5 μm were placed at different distances from the center of the gasket hole in order to evaluate the pressure gradient in the chamber. The accuracy in pressure measurements and pressure variations within the cell was ~0.2 GPa.

The room-temperature synchrotron Mössbauer experiments (NFS) were performed on the $Ba_3TaFe_3Si_2O_{14}$ samples at high pressures up to 49.4 GPa, and the low-temperature experiments—at pressure up to ~38 GPa. At every temperature scan, the NFS spectra were measured in the temperature region from ~20 to 300 K. The measurements were done with the nuclear resonant scattering equipment at the 16ID-D beam-line at the Advanced Photon Source (APS, Argonne, USA) in 24-bunch mode.

Raman scattering measurements were made at room temperature at pressures up to ~30 GPa at both compression and decompression cycles.

The high-pressure evolution of Raman spectra of $Ba_3Ta^{57}Fe_3Si_2O_{14}$ shown in Fig. 2(a) reveals small changes in shape of the spectra at ~6.8 GPa and a drastic change in the spectra between 19.5 and 20.3 GPa. At $P > 20.3$ GPa, the sharp peaks completely disappear transforming into two very broad maxima. Pressure behaviour of Raman peaks positions demonstrates more clearly the appearance of successive transitions at ~6.8 and 19.5 GPa (Fig. 2(c)). During decompression (Figs. 2(b) and 2(d)), we observed large hysteresis (of about 16 GPa) which is indicative of a first-order type of the structural phase transition with a large energy barrier between low- and high-pressure phases. The Raman spectra above 19.5 GPa are much broader, which may be related to the small grain size and possibly even to amorphous structure of the high-pressure phase. At decompression to ambient pressure, Raman spectral shape returns to original sharp peaks characteristic of the low-pressure (LP) crystalline structure. These findings support the diffuse-like transition of the first order type with strong reconstruction of crystalline structure possibly involving large volume effect. This picture is also supported by the large hysteresis of the inverse transition at decompression.

The possible structural transitions in langasite family crystals were considered and observed experimentally in Ref. 25. In particular, the change of trigonal symmetry (sp. gr. $P321$) into monoclinic (sp. gr. $A2$-$C2$) was found in $La_3SbZn_3Ge_2O_{14}$ at temperature decrease as well in $La_3Nb_{0.5}Ga_{5.5}O_{14}$ and $La_3Ta_{0.5}Ga_{5.5}O_{14}$ crystals under high pressure of ~12 GPa.[26] It was shown that the lowering symmetry transitions $P321 \rightarrow P3$ and $P321 \rightarrow C2$ are the most probable in the langasite family.

The room temperature evolution of NFS spectra in $Ba_3Ta^{57}Fe_3Si_2O_{14}$ at high pressures is shown in Fig. 3(a).

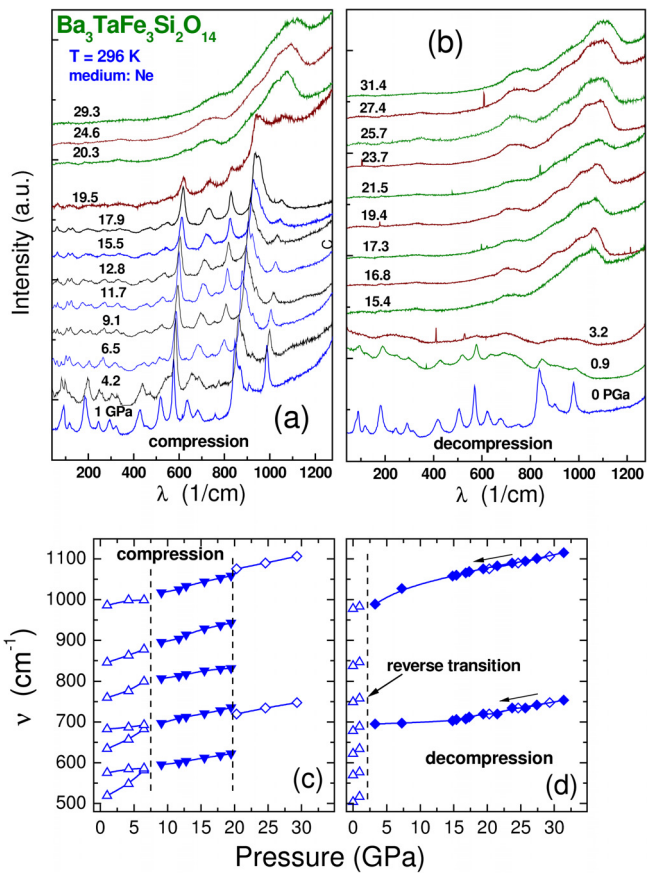

FIG. 2. The pressure evolution of Raman spectra of the $Ba_3TaFe_3Si_2O_{14}$ (50% Fe-57) sample at room temperature: (a) compression, (b) decompression. The pressure dependences of the most intense Raman peaks at compression (c) and decompression (d). Two anomalies at ~6.8 and ~19.5 GPa imply structural transitions. The hysteresis of about ~17 GPa at decompression is a signature of a first-order type transition with a large volume drop. The pressure medium was Ne.

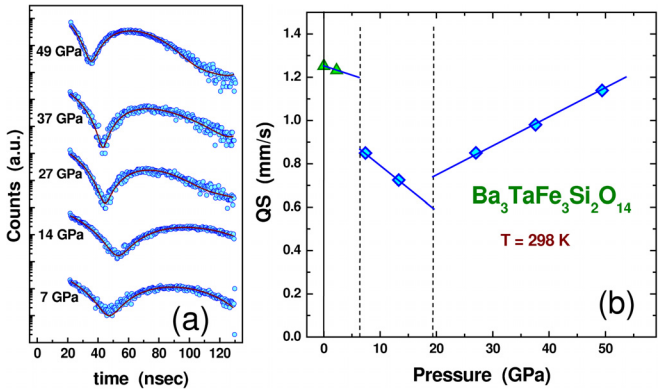

FIG. 3. The evolution of NFS spectra of the $Ba_3TaFe_3Si_2O_{14}$ (50% Fe-57) sample during compression at room temperature (a). The pressure dependence of QS at ^{57}Fe nuclei (b) calculated from the NFS spectra: rhombic symbols. The pressure medium was He. The QS values at pressures between ambient and 6.5 GPa we determined from the Mössbauer absorption measurements (triangle-up symbols).

The quadrupole splitting (QS) values calculated from the spectra reveal a drastic stepwise changes at pressures of ~6.8 and ~20 GPa (see Fig. 3(b)), which correlates with possible structural transitions observed in the Raman scattering experiments.

The QS value drops down from ~1.2 mm/s to ~0.9 mm/s indicating the first transition at ~6.8 GPa. Then QS decreases from ~0.9 to ~0.6 mm/s in the region 6.8–20 GPa, and starts to increase again at $P > 20$ GPa indicating the second transition. After transition at ~20 GPa, the QS value increases linearly to ~1.17 mm/s at ~50 GPa. It should be noted that in addition to the stepwise jump of the QS value at the transitions, the pressure slope of QS converts from negative to positive sign after the transition at 19.5 GPa.

The NFS spectra of nuclear resonance forward scattering from ^{57}Fe nuclei in $Ba_3TaFe_3Si_2O_{14}$ recorded at selected pressures in the temperature (T) region between 20 and 300 K are shown in Fig. 4. The spectra represent the intensity of scattered synchrotron radiation depending on the time after SR pulse. In our experiment, we have optimised the thickness of the sample to have only quantum-beats[27] in the time spectra (see optimisation procedure in Ref. 28). The NFS spectra were processed by the MOTIF program developed by Shvyd'ko.[29]

As shown in Fig. 4, the high-frequency quantum beats of the magnetic nature are present in the spectra at low T indicating the magnetic ordering of the iron ions. With T increase, only low-frequency quantum beats can be seen in the NFS spectra, revealing the paramagnetic state (Fig. 4). Disappearance of the magnetic quantum beats at certain T indicates the transition from the magnetically ordered state to the paramagnetic state. Based on the analyses of the NFS spectra, we have derived the Néel temperatures T_N of the sample at each pressure.

The low-frequency quantum beats appear to be a result of the electric quadrupole interaction of the ^{57}Fe nuclei with the electric field gradient at the local iron sites. The quality of NFS spectra in paramagnetic state above T_N provides enough accuracy to determine the QS of the nuclear levels. We have found that the one-doublet model of the spectra gives good fitting result in accordance with the Mössbauer

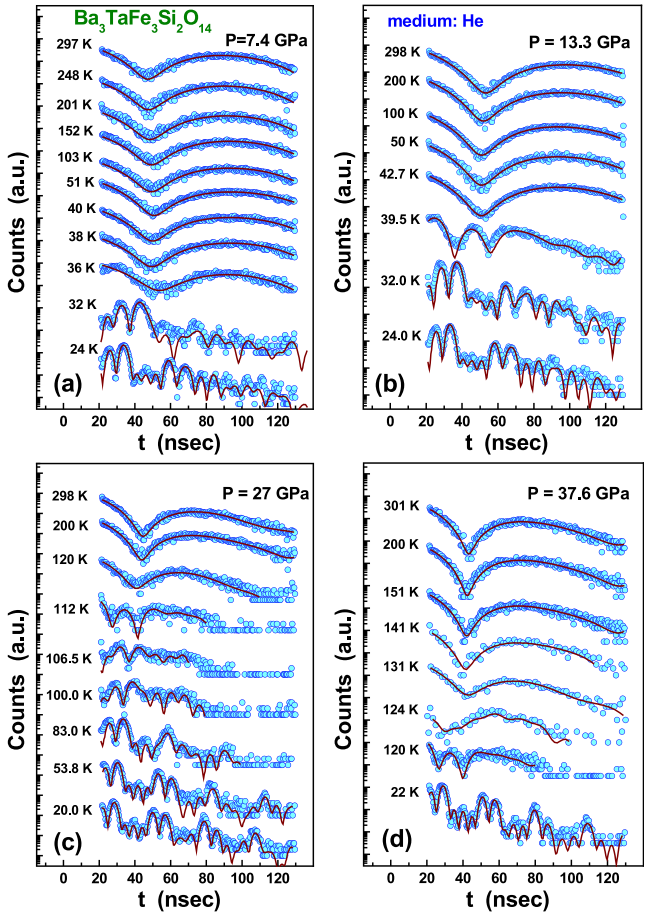

FIG. 4. The temperature evolution of NFS spectra of the $Ba_3TaFe_3Si_2O_{14}$ (50% Fe-57) powder sample at several fixed pressures. Symbols are the experimental points; solid lines are the result of fitting to the MOTIF model. The pressure medium was He.

transmission spectra studies.[2] However, the fitting of the spectra in the antiferromagnetic state below T_N is not a simple task. As was found in Ref. 2, the iron sites in $Ba_3TaFe_3Si_2O_{14}$ are split into two or more magnetic sublattices at $T < T_N$, and the resonance lines are broaden due to distribution of magnetic hyperfine field H_{hf} at iron nuclei in non-equivalent positions. Our NFS spectra also indicate a narrow but detectable distribution of the H_{hf} values. The MOTIF program is not developed enough for powder samples when a distribution of the H_{hf} values and directions needs to be taken into account. However, we found that the use of 4-sextets model for the simulation of the H_{hf} distribution allow to obtain the average values of the field $\langle H_{hf} \rangle$ with rather high accuracy (with an error of ~2 Tesla). This error is comparable with the symbol sizes in the Fig. 5. The $\langle H_{hf} \rangle$ values calculated for different pressure-temperature conditions are shown in Fig. 5.

Previously, we have shown[12] that the dependence of T_N on pressure can be calculated from an empirical function which describes the pressure-temperature dependence of the field $H_{hf}(P, T)$,

$$H_{hf}(P,T) = H_{hf}(P,0) \times \exp\left(-\alpha \frac{T}{T_N(P)}\right) \times \left[1 - \frac{T}{T_N(P)}\right]^{\beta}. \quad (1)$$

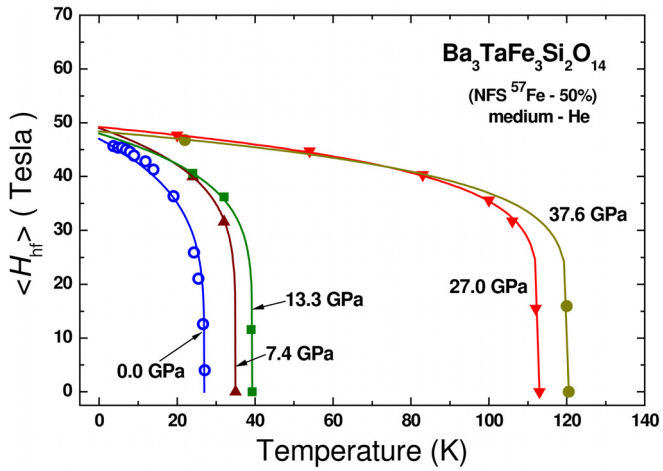

FIG. 5. The evolution of temperature dependence of magnetic hyperfine field $\langle H_{hf}\rangle$(T) at pressure increase. Symbols are the experimental values of $\langle H_{hf}\rangle$ obtained from NFS spectra of Fig. 2. Solid lines are the empirical analytical function (Eq. (1)) fitted to experimental points.

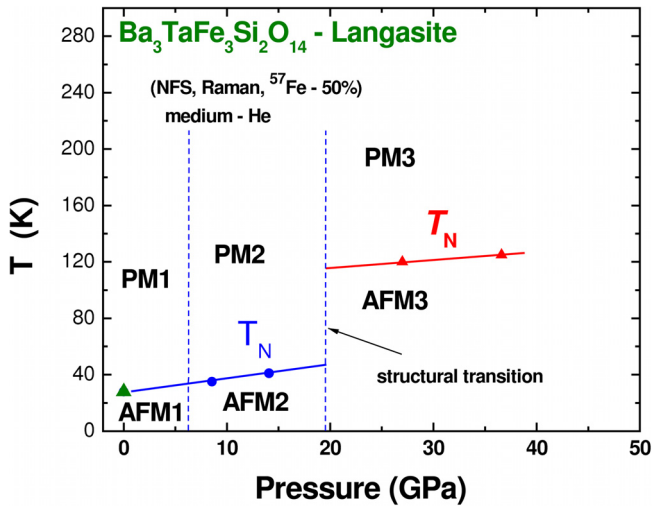

FIG. 6. The tentative magnetic P-T phase diagram of langasite $Ba_3TaFe_3Si_2O_{14}$ (50% Fe-57) at hydrostatic compression up to ~38 GPa. The dashed vertical lines indicate structural transitions at pressure increase. The triangle-up symbol at P = 0 GPa is the Neel temperature obtained at ambient pressure from the Mössbauer absorption measurements (Ref. 6).

Here, $H_{hf}(P,0)$ is the pressure dependence of H_{hf} at zero temperature, α and β are the parameters of the empirical function which can be found from the fit of Eq. (1) to the experimental dependence H_{hf}(T). From our previous precise Mössbauer measurements,[2] we know the value of $H_{hf}(0,0) = 45.0$ Tesla, the exact behaviour $H_{hf}(T)$ at $P = 0$, and the value of $T_N(P = 0) = 27.2$ K. Fitting the $H_{hf}(T,0)$ curve to Eq. (1) gives $\alpha = 0.01$ and $\beta = 0.21$.

From NFS data, we have found that the parameters of the empirical function (Eq. (1)) are $\alpha = 0.01$ and $\beta = 0.17$ for the low-pressure phase (at $P < \sim 19.5$ GPa), whereas $\alpha = 0.01$ and $\beta = 0.145$ for the high-pressure phase (at $P > 20$ GPa).

The fits of empirical function (Eq. (1)) to experimental points for every pressure are shown by solid lines in Fig. 5. It was found that there is a very weak pressure dependence of the H_{hf}(T = 0 K) value. Extrapolation of all fits in Fig. 5 to $T = 0$ K gives values of the magnetic hyperfine field H_{hf} (T = 0 K) = 48 ± 1 Tesla.

Thus, we have established that the T_N value gradually increases from 27.2 to 41 K at pressure rise from ambient to $P = 19.5$ GPa, and then it dramatically jumps up to 120 K as the result of the structural transition. Evidently, it can be explained by large sensitivity of super-exchange interaction to the structural reorganization of $Ba_3Ta^{57}Fe_3Si_2O_{14}$. The pressure slopes of T_N before and after structural transition at 19.5 GPa are ~0.97 K/GPa and ~0.49 K/GPa, respectively.

On the basis of obtained data, we plot a tentative magnetic P-T phase diagram (Fig. 6), which shows various magnetic states of $Ba_3TaFe_3Si_2O_{14}$ at different pressures and temperatures. The dashed vertical lines at $P = 6.8$ and 19.5 GPa and solid lines separate the paramagnetic PM1 and PM2 and antiferromagnetic AFM1 and AFM2 phases in "LP" region ($P < 19.5$ GPa). At $P > 19.5$ GPa, a paramagnetic PM3 and antiferromagnetic AFM3 phases occur in the HP phase. The solid lines in Fig. 6 separate the antiferromagnetic (AF) and the paramagnetic (PM) states developing at $T < T_N$ and $T > T_N$, respectively.

One of the fundamental problems in the high-pressure investigations is a search for possible spin crossover transition at iron ions Fe^{3+} from the high-spin (HS, S = 5/2) to the low-spin (LS, S = 1/2) state.

Such a transition was observed and explained in many experimental and theoretical studies for octahedrally coordinated Fe^{3+} ions in many oxides,[21] with notable exception of spinel-type structures with much smaller octahedra at ambient conditions, where lower-pressure spin transitions have been observed.[30,31]

In the langasite-type crystals iron ions occupy the tetrahedral oxygen sites, and it is important to find out—what pressure should be expected for the spin-crossover transition in such materials?

To calculate the effective Hubbard parameter U^{eff} at different pressures, we take $U^{eff}{}_{HS} = E_{HS}(d^4) + E_{HS}(d^6) - 2E_{HS}(d^5)$ at $P < P_c$, and $U^{eff}{}_{LS} = E_{LS}(d^4) + E_{LS}(d^6) - 2E_{LS}(d^5)$ at $P > P_c$. Where $E_{HS,LS}(d^4)$, $E_{HS,LS}(d^5)$ and $E_{HS,LS}(d^6)$ – are the HS and LS terms for d^4, d^5 and d^6 configurations respectively, and P_c – is the pressure value of spin-crossover transition.

For tetrahedral sites, we calculate the *HS* and *LS* terms using methods outlined in Refs. 15, 32, and 33. Calculation details can be found in Supplementary Materials (see Ref. 34). Finally,

$$\begin{aligned} U^{eff}{}_{HS} &= U + 4J - 10Dq(P) \quad \text{at } P < P_c, \\ U^{eff}{}_{LS} &= U \qquad\qquad\qquad\qquad \text{at } P > P_c. \end{aligned} \tag{2}$$

Thus, $U^{eff}{}_{HS}$ linearly decreases down to $(U + J)$ at $P = P_c$, then it drops down to $U^{eff}{}_{LS} = U$ at $P > P_c$.

These calculations show that for the tetrahedral sites, one has the effect of decreasing correlations under pressure similar to that in the octahedral sites.

The important result of our consideration is almost one order of magnitude higher value for the pressure of the spin-crossover in tetrahedral sites with respect to the octahedral sites. Nevertheless, there are several other possibilities of the HS → LS spin-crossover in tetrahedral position. One of the possibilities is the structural transition with re-coordination of iron ions from tetra- to octa-environment of ligands. If

such a transition would occur at pressures 40–70 GPa or higher, it could initiate the immediate HS → LS spin-crossover in electronic system of Fe^{3+} ions.

We have investigated the high-pressure properties of the langasite type $Ba_3Ta^{57}Fe_3Si_2O_{14}$ compound in hydrostatic pressures up to 38 GPa and at low temperatures down to 20 K. At pressures ~19.5 GPa, a magnetic transition with huge increase in the Neel temperature was observed. Relative to the ambient pressure, the T_N value is increased by about a factor of four (from 27.2 to 120 K). The structural transition at ~19.5 GPa, revealed by Raman spectroscopy, is most likely a first-order type transition. This conclusion is supported by the drastic change of Raman spectra and by the large hysteresis of the inverse transition at decompression. Strong pressure dependence of T_N could be explained by high sensitivity of super-exchange interaction to compression. This sensitivity could be explained by a strong dependence of super exchange on bond-angle, which changes substantially at the structural transition. Preliminary theoretical consideration predicts much higher pressure value of the spin-crossover transition $HS(S = 5/2) \rightarrow LS(S = 1/2)$ for tetrahedron environment (about 800 GPa) in comparison with octahedron environment (about 70 GPa).

Up to date, only few multiferroic crystals have parameters appropriate for practical use, therefore, any possibility to find another materials suitable for applications is important. We have demonstrated a possibility of drastic increase (almost 4 times) of the Neel temperature in langasite due to structural change induced by modest pressure. In principle, there is a possibility to find a chemical composition that would influence the crystals by imposing "chemical" pressure or find a thin film substrate capable of inducing stresses sufficient to induce high values of T_N. Our results may help to understand how the langasite structure could be modified by chemical engineering to increase critical temperatures, thus creating materials of practical importance.

We deeply thank Dr. B. V. Mill and Dr. P. G. Naumov for the synthesis the $Ba_3TaFe_3Si_2O_{14}$ sample with ^{57}Fe isotope. The work was supported as part of the EFRee, an Energy Frontier Research Center funded by the U. S. Department of Energy, Office of Science. This work was also supported by the Russian Foundation for Basic Research (Grant Nos. 13-02-12419-ofi-m, 11-02-12089, 11-02-00291-a, 14-02-01033-a, 14-02-00483-a, and 13-02-00358-a), by RAS programs "Strongly correlated electron systems," "Elementary particle physics, fundamental nuclear physics and nuclear technologies," and Russian Ministry of science and education Program "Kadry," GK 16.740.11.0740, and Siberian Federal University Grant F11. VVS and AGG acknowledge support from DOE (Grant #DE-FG02-02ER45955) and CDAC/NNSA. Portions of this work were performed at HPCAT (Sector 16), Advanced Photon Source (APS), Argonne National Laboratory. HPCAT operations are supported by DOE-NNSA under Award No. DE-NA0001974 and DOE-BES under Award No. DE-FG02-99ER45775, with partial instrumentation funding by NSF. APS is supported by DOE-BES, under Contract No. DE-AC02-06CH11357.

[1]B. V. Mill', E. L. Belokoneva, and T. Fukuda, Russ. J. Inorg. Chem. **43**, 1168 (1998).
[2]I. S. Lyubutin, P. G. Naumov, and B. V. Mill', EPL **90**, 67005 (2010).
[3]B. V. Mill and Y. V. Pisarevsky, paper presented at the 2000 IEEE/EIA International Frequency Control Symposium, Kansas City, MO, 2000.
[4]E. L. Belokoneva and N. V. Belov, Dokl. Akad. Nauk SSSR **260**, 1363 (1981).
[5]B. V. Mill, A. V. Butashin, G. G. Kodzhabagyan, E. L. Belokoneva, and N. V. Belov, Dokl. Akad. Nauk SSSR **264**, 1395 (1982).
[6]I. S. Lyubutin, P. G. Naumov, B. V. Mill', K. V. Frolov, and E. I. Demikhov, Phys. Rev. B **84**, 214425 (2011).
[7]K. Marty, P. Bordet, V. Simonet, M. Loire, R. Ballou, C. Darie, J. Kljun, P. Bonville, O. Isnard, P. Lejay, B. Zawilski, and C. Simon, Phys. Rev. B **81**, 054416 (2010).
[8]K. Marty, V. Simonet, P. Bordet, R. Ballou, P. Lejay, O. Isnard, E. Ressouche, F. Bourdarot, and P. Bonville, J. Magn. Magn. Mater. **321**, 1778 (2009).
[9]K. Marty, V. Simonet, E. Ressouche, R. Ballou, P. Lejay, and P. Bordet, Phys. Rev. Lett. **101**, 247201 (2008).
[10]S. A. Pikin and I. S. Lyubutin, Phys. Rev. B **86**(6), 064414 (2012).
[11]M. Loire, V. Simonet, S. Petit, K. Marty, P. Bordet, P. Lejay, J. Ollivier, M. Enderle, P. Steffens, E. Ressouche, A. Zorko, and R. Ballou, Phys. Rev. Lett. **106**, 207201 (2011).
[12]A. G. Gaviliuk, I. A. Trojan, I. S. Lyubutin, V. A. Sarkissian, and S. G. Ovchinnikov, JETP **100**(4), 688–696 (2005).
[13]A. G. Gavriliuk, I. A. Trojan, R. Boehler, M. I. Eremets, I. S. Lubutin, and N. R. Serebrianaya, JETP Lett. **77**(11), 619–624 (2003).
[14]A. G. Gavriliuk, S. A. Kharlamova, I. S. Lyubutin, I. A. Trojan, S. G. Ovchinnikov, A. M. Potseluyko, M. I. Eremets, and R. Boehler, JETP Lett. **80**(6), 426–432 (2004).
[15]A. G. Gavriliuk, V. V. Struzhkin, I. S. Lyubutin, and I. A. Trojan, JETP Lett. **82**(9), 603–608 (2005).
[16]I. S. Lyubutin, A. G. Gavriliuk, I. A. Trojan, and R. A. Sadykov, JETP Lett. **82**(11), 702–707 (2005).
[17]I. S. Lyubutin, A. G. Gavriliuk, V. V. Struzhkin, S. G. Ovchinnikov, S. A. Kharlamova, L. N. Bezmaternykh, M. Hu, and P. Chow, JETP Lett. **84**(9), 518–523 (2007).
[18]A. G. Gavriliuk, I. A. Trojan, and V. V. Struzhkin, Phys. Rev. Lett. **109**, 086402 (2012).
[19]A. G. Gavriliuk, V. V. Struzhkin, I. S. Lyubutin, S. G. Ovchinnikov, M. Y. Hu, and P. Chow, Phys. Rev. B **77**, 155112 (2008).
[20]I. S. Lyubutin, A. G. Gavriliuk, and V. V. Struzhkin, JETP Lett. **88**(8), 524–530 (2008).
[21]I. S. Lyubutin and A. G. Gavriliuk, Phys. Usp. **52**(10), 989–1017 (2009).
[22]I. S. Lyubutin, A. G. Gavriliuk, K. V. Frolov, J.-F. Lin, and I. A. Trojan, JETP Lett. **90**(9), 617–622 (2010).
[23]I. S. Lyubutin, S. G. Ovchinnikov, A. G. Gavriliuk, and V. V. Struzhkin, Phys. Rev. B **79**(8), 085125 (2009).
[24]A. G. Gavriliuk, A. A. Mironovich, and V. V. Struzhkin, Rev. Sci. Instrum. **80**, 043906 (2009).
[25]B. V. Mill', B. A. Maksimov, Y. V. Pisarevsky, N. P. Daniliva, A. Pavlovska, S. Werner, and J. Schneider, Crystallogr. Rep. **49**, 60 (2004).
[26]A. Pavlovska, S. Werner, B. Maximov, and B. Mill, Acta Crystallogr. **58**, 939–947 (2002).
[27]G. V. Smirnov, Hyperfine Interact. **123/124**, 31 (1999).
[28]A. G. Gavriliuk, J. F. Lin, I. S. Lyubutin, and V. V. Struzhkin, JETP Lett. **84**(3), 161–166 (2006).
[29]Y. V. Shvyd'ko, Phys. Rev. B **59**, 9132 (1999).
[30]Y. Ding, D. Haskel, S. G. Ovchinnikov, Y.-C. Tseng, Y. S. Orlov, J. C. Lang, and H.-K. Mao, Phys. Rev. Lett. **100**, 045508 (2008).
[31]T. Yamanaka, A. Kyono, Y. Nakamoto, Y. Meng, S. Kharlamova, V. V. Struzhkin, and H.-K. Mao, Am. Mineral. **98**, 736–744 (2013).
[32]Y. Tanabe and S. Sugano, J. Phys. Soc. Jpn. **9**, 753–766 (1954).
[33]S. G. Ovchinnikov, JETP **107**, 140 (2008).
[34]See supplementary materials at http://dx.doi.org/10.1063/1.4822422 for details of theoretical calculations.